Analytical Honeycomb Geometry for Raster and Volume Graphics

Valentin E. Brimkov* Reneta P. Barneva†

Abstract

In this paper we investigate the advantages of using hexagonal grids in raster and volume graphics. In 2D, we present a *hexagonal graphical model* based on a hexagonal grid. In 3D, we introduce two *honeycomb graphical models* in which the voxels are hexagonal prisms, and we show that these are the only possible models under certain reasonable conditions. In the framework of the proposed models, we design two- and three-dimensional *analytical honeycomb geometry* of linear objects, as well as of circles and spheres. We demonstrate certain advantages of the honeycomb models and address algorithmic and complexity issues.

Keywords: *Raster graphics, Volume graphics, Digital geometry, Analytical digital geometry, Tiling, Square grid, Cubic grid, Hexagonal grid, Honeycomb model*

1 Introduction

Various advantages of volume graphics over surface graphics have been widely discussed in the literature (see, e.g., [17]). However, certain disadvantages of the former have been quite early recognized. One can list the following, among others [17]:

- *Loss of geometric information* after voxelization of a surface object. The voxels composing a digital surface do not retain the geometric information contained in the definition of the surface.

- *High aliasing artifacts* due to the discrete nature of the data from which the continuous object is reconstructed (such as appearance of holes in the object after performing some operations).

- *Large amount of memory and computational resources* are required in order to store and manipulate digital objects.

Over the last decades, numerous useful theoretical results have been obtained in *digital topology* and *digital geometry*. These are disciplines providing theoretical foundations for computer graphics and digital image analysis (see [15, 16, 19, 23, 29]). A promising approach which may help resolve problems such as those listed above, is based on developing an *analytical digital geometry* (see, e.g.,

*Department of Mathematics and Computer Science, State University of New York, Fredonia, NY 14063, USA. E-mail: brimkov@cs.fredonia.edu. Part of this work has been done while this author was visiting the Laboratory on Signal, Image and Communication, IRCOM, Université de Poitiers, Poitiers, France, and Dipartimento di Elettronica ed Informatica, Università di Padova, Italy

†Department of Mathematics and Computer Science, State University of New York, Fredonia, NY 14063, USA. E-mail: barneva@cs.fredonia.edu. Part of the work has been done while this author was visiting the Multimedia Laboratory of Dipartimento di Elettronica ed Informatica, Università di Padova, Italy, and the Computer Graphics Group of IEI-CNR Pisa, Italy.

[6] for introduction). The main objective here is to obtain simple analytical description of the basic Euclidean primitives and to develop algorithms for modeling using such primitives.

Digital geometry (as well as analytical digital geometry) deals with geometrical properties of "digital images," which are sets of points of the digital space $\mathbb{Z}^n$. The raster computer graphics is modeled upon a regular square grid, where the square tiles are called *pixels*. Square grids are physically implemented in computer displays. In dimension three, the graphical models are based on regular cubic tilings, in which the cubes are called *voxels*. Alternatives to the square/cubic grid have also been considered. In 2D, such an alternative is provided by the hexagonal grid whose cells are regular hexagons. Certain properties of hexagonal tilings of the plane have been first studied in relation with research on covering and packing of the plane. Studies on these last topics seem to originate from a work of Gauss from 1831 introducing the idea of lattice. Over the years, contribution to the subject have been made by mathematicians like Minkowski, Davenport and Rogers, among others. See the classical monograph of Rogers [22] for historical and other details related to this early stage. In particular, one can see that regular hexagons provide economic (and under certain conditions optimal) plane covering and packing. Hexagonal rasters are well-known in image processing (see, e.g., [14, 27]). Recent works elucidate various interesting points. For instance, algorithmic comparison between hexagonal- and square-based models is available in [30]. This last work also provides a discussion on the possibility of implementing hexagonal grids to graphical devises. [31, 32] present algorithms for drawing lines and circles.

Alternatives to the cubic grid in 3D have also been considered. Some properties and advantages of grids based on truncated dodecahedral or rhombic dodecahedral tilings have been studied, e.g., in [20, 13].

In the present paper we consider the case when the tile is a hexagonal prism. We call the corresponding models the "3D honeycomb models." To our knowledge of the available literature, such kind of models have not been seriously studied, although they indeed expose certain advantages over the classical cubic model. In brief, we show that the honeycomb models ensure tunnel-freedom of digital objects in a more direct way than the cubic models. Moreover, they ensure better approximation to a continuous object (in terms of Hausdorff distance) and in some regards are "more economic." The proposed honeycomb models employ simple mathematics and provide possibilities for a straightforward transfer of notions and results from the classical digital geometry.

Our main contribution is developing analytical honeycomb geometry of some fundamental Euclidean primitives, such as straight lines, segments, polygons, circles, planes, spheres, etc. Their simple analytical description straightforwardly provides simple drawing algorithms. Our analytical approach makes the theoretical considerations either obvious or rather simpler than those of [31, 32].

The paper is organized as follows. In the next section we recall some definitions and introduce notions to be used in the sequel. In Section 3, we provide theoretical foundations for developing 2D digital analytical honeycomb geometry of linear objects and circles. We also discuss on some advantages of the hexagonal grid. In Section 4, we extend our considerations to the 3D space by introducing two honeycomb graphical models in which the voxels are hexagonal prisms. We show that these are the only possible models under certain reasonable conditions. We also develop analytical digital honeycomb geometry within these models. In Section 5, we address algorithmic and complexity issues. We conclude with some final remarks in Section 6.

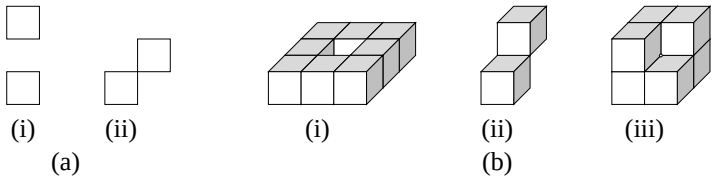

Figure 1: Different types of tunnels in the case of square/cubic tiles: a) Tunnels in a 2D digital object. (i) 1-tunnel, (ii) 0-tunnel. b) Tunnels in a 3D object: (i) 2-tunnel, (ii) 1-tunnel, (iii) 0-tunnel.

2 Preliminaries

2.1 Basic Notions of Digital Topology and Geometry

A tiling $\mathcal{P}$ of $\mathbb{R}^n$ by convex polytopes is called *normal* [26] if the intersection of any two tiles from $\mathcal{P}$ is either empty or appears to be their common $(n-d)$-dimensional facet, for some d, $1 \leq d \leq n$.

Let $\mathcal{T}$ be a normal tiling of $\mathbb{R}^n$, $n = 2$ or 3, where the tiles P of $\mathcal{T}$ are convex polytopes. For a set of tiles A we denote $U(A) = \cup_{P \in A} P$. A set of tiles will be regarded as a *digital object*. A j-dimensional facet of a tile $P \in \mathcal{T}$ is called *j-facet*, for some j, $0 \leq j \leq n-1$. Thus the 0-facets of P are its vertices, the 1-facets are its edges, and the 2-facets of a 3D polytope are its 2D faces. Two tiles are called *j-adjacent* if they share a j-facet. A *k-path* in a digital object A is a sequence of tiles from A such that every two consecutive tiles are k-adjacent. Two tiles are *k-connected* if there is a k-path between them. A digital object A is *k-connected* if there is a k-path connecting any two tiles of A. A digital object is *connected* if it is at least 0-connected. Otherwise it is *disconnected*.[1] A *k-component* of a digital object A is a maximal (non-extendable) k-connected set of tiles of A.

Let D be a subset of a digital object A. If $A - D$ is not k-connected then the set D is called *k-separating* in A. Let a set of tiles A be k-separating in a digital object B but not j-separating in B. Then A is said to have j-tunnels for any $j < k$. Digital object without k-tunnels is called *k-tunnel-free*. An object that has no tunnels for any k, $0 \leq k \leq 2$, is called *tunnel-free*, for short.[2]

The notion of tunnel plays an important role in rendering voxelized scenes by casting digital rays from the image to the scene [9]. Since thinner rays are much more attractive for ray traversal, it is desirable to construct k-tunnel-free digital objects where k is as small as possible. In 2D, the connectivity of a digital object fully characterizes the topology of the tunnels. More precisely, an object A contains 1-tunnels iff it is disconnected; A contains 0-tunnels but no 1-tunnels iff it is connected but not 1-connected; and A is tunnel-free iff it is 1-connected. In dimension 3, however, the situation is more complicated. The variety of possibilities may cause certain difficulties when constructing k-tunnel-free discretizations of more complex objects. Thus, it may be difficult to control the object connectivity. Moreover, it might even be a problem to secure that a digital object is connected [6]. Ensuring tunnel-freedom can be a difficult task as well [6, 8, 7]. A source for these difficulties is the

[1] Classically, 0-adjacent/connected (resp. 1-adjacent/connected) pixels are called 8-adjacent/connected (resp. 4-adjacent/connected). In dimension 3, 0-adjacent/connected (resp. 1 or 2-adjacent/connected) voxels are called 26-adjacent/connected (resp. 18 or 6-adjacent/connected).

[2] Classically, in dimension two, a 0-tunnel (resp. 1-tunnel) is called 8-tunnel (resp. 4-tunnel). In dimension three, a 0-tunnel (resp. 1- or 2-tunnel) is called 26-tunnel (resp. 18- or 6-tunnel).

topology of the square grid. In Sections 4 and 5 we will see how they can be easily overcome by using honeycomb models.

The notion of tunnels is closely related to the one known in digital topology as "good pairs" of adjacency relations (see, e.g., [18, 25]). The latter arises in particular when one works with closed digital curves (in 2D) and closed digital surfaces (in 3D). It turns out that in order to make the considerations meaningful, one should use different topologies when dealing with the curve/surface or with its complement. For instance, the following discrete version of the well-known Jordan curve theorem has been proved [24]:

Theorem 1 *If C is the set of points of a simple closed 1-curve (0-curve) and $|C| > 4$ ($|C| > 3$), then the complement $\overline{C}$ of C has exactly two 0-components (1-components).*

In this context, (1,0) and (0,1) are *good pairs* of adjacency relations, while (1,1) and (0,0) are not. Similar situation takes place in 3D: (2,0), (0,2), (2,1), and (1,2) are good pairs, while (2,2), (1,1), and (0,0) aren't. Thus, it is necessary to use different adjacencies when processing a digital object and its complement. However, if one uses a hexagonal grid with an adjacency relation μ defined by nearest neighbor, such an undesirable asymmetry does not exist anymore as (μ, μ) turns out to be a good pair [18].

2.2 Analytical Digital Geometry

In recent years, *analytical digital geometry* has been developed by several authors (see [21] and the bibliography in [12],[2]). This approach is very successful especially when dealing with linear objects. Analytical descriptions and based on them efficient digitization algorithms have been obtained for 2D and 3D digital straight lines or their segments [21, 11, 7, 5], digital planes [21, 10, 3, 5], 2D and 3D digital polygons, as well as tunnel-free meshes of 3D polygons [4, 6, 8, 7]. These results are of significant practical importance since for various applications it suffices to work with a reasonable polyhedral approximation to the given real object. Circles and spheres have been analytically defined as well [1]. As an illustration we recall the analytical definition of a digital straight line.

2D arithmetic line is a set of pixels $L(a_1, a_2, \mu, \omega) = \{(x, y) \in \mathbb{Z}^2 | 0 \leq a_1 x + a_2 y + \mu < \omega\}$, where $a_1, a_2, \mu \in \mathbb{Z}$, $\omega \in \mathbb{N}$. ω is called *arithmetic thickness* or *width* of the line and μ is its *intercept*. The vector (a_1, a_2) is the *normal vector* to the line. An arithmetic line $L(a_1, a_2, \mu, \omega)$ is *0-connected* (classically, *8-connected* or *naive*) if $\omega = \max(|a_1|, |a_2|)$, and *1-connected* (classically, *4-connected* or *standard*), if $\omega = |a_1| + |a_2|$. The standard line is the thinnest tunnel-free arithmetic line. Analytical digital plane is defined analogously.

The analytical approach to raster and volume graphics may lead to important advantages. The analytical digital geometry is purely discrete and involves simple integer arithmetics. A digital object is compactly defined by formulas which may help achieve a very economic object encoding. Analytical definition may help achieve better accuracy of certain operations, for which one can take advantage of the corresponding analytical formulas used in the definition. Note also that after performing voxelization, the distinct voxels still retain certain information about the original object. In particular, it is usually straightforward to determine whether a voxel belongs to an analytical digital object, to its interior or boundary, or to the intersection or the union of two or more analytically defined objects.

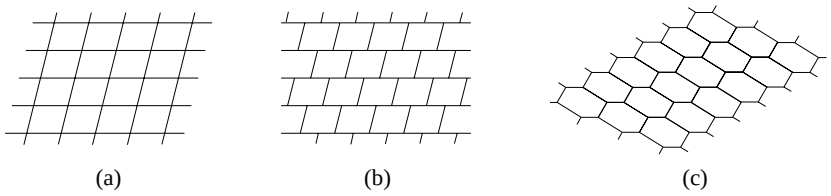

Figure 2: a) Tiling by a parallelogram. b) Brick-built tiling. c) Tiling by a quasi-regular hexagon.

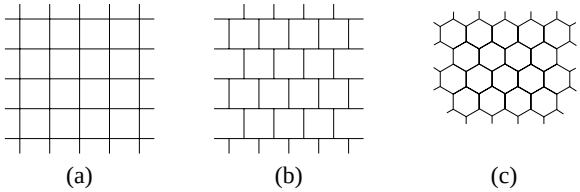

Figure 3: a) Square grid. b) Regular brick-built grid. c) Regular hexagonal grid.

Moreover, negative effects and phenomena like object disconnectedness or appearance of holes and tunnels can be understood more deeply and as a result avoided.

2.3 Hexagonal and Honeycomb Tilings

Consider a normal tiling $\mathcal{P}$ of $\mathbb{R}^n$, $n = 2$ or 3, by copies of the same tile P, so that the following conditions are met: (i) P is a convex set, (ii) For any $P_1, P_2 \in \mathcal{P}$ there is a translation τ such that $\tau(P_1) = P_2$, and (iii) If p is a point of a tile $P \in \mathcal{P}$, then the set of the duplicas of p in all tiles from $\mathcal{P}$ is a lattice in $\mathbb{R}^n$. A tiling with these properties is called a *uniform tiling*.

First we consider uniform tilings of $\mathbb{R}^2$. It is well-known (and also easy to see) that a uniform tiling is possible only if the tile P is a parallelogram (Figure 2a,b) or a hexagon whose opposite sides are equal and parallel (Figure 2c). Such a hexagon is called *quasi-regular*. The vertices and sides of the tiles form a *grid*. The *center* of a tile is the intersection point of its diagonals. Sometimes we will identify a tile with its center. A grid can be regarded as an infinite plane graph $G = (V, E)$ whose vertex set V and edge set E consist of the polygons' vertices and sides, respectively. Note that the graph of the hexagonal grid of Figure 2c is isomorphic to the one of the parallelogram tiling of Figure 2b. Thus, these two grids have the same topology, despite the different shape of their tiles. A tiling/grid as the one in Figure 2b will be called a *brick-built tiling/grid*. If we require the tiles to be regular polygons, then we obtain the *square tiling/grid* depicted in Figure 3a, the *regular brick-built tiling/grid* in Figure 3b, and the *regular hexagonal tiling/grid* in Figure 3c.

As already mentioned, $\mathbb{R}^3$ can be uniformly tiled by parallelepiped, truncated dodecahedron, rhombic dodecahedron, or hexagonal prism. In what follows, we will study and compare models on grids generated by a tile P that is either a parallelepiped or a hexagonal prism whose bases are quasi-regular hexagons. The notions of a grid and a tile center are defined analogously to the 2D case.

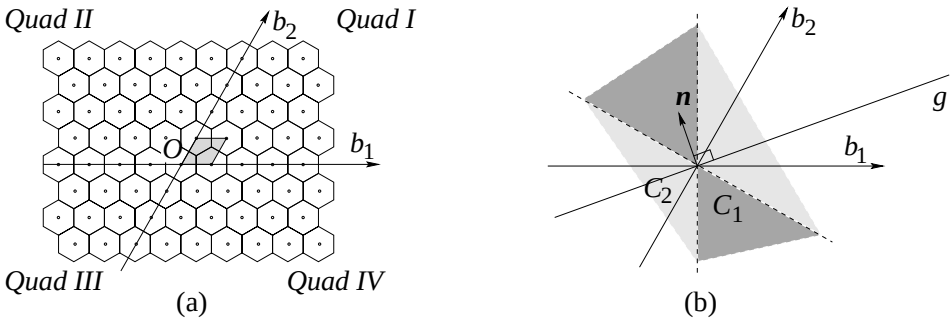

Figure 4: a) Hexagonal coordinate system and Quad I,II,III,IV. b) The cones C_1 and C_2. The normal vector $\mathbf{n} = (a_1, a_2)$ to the straight line g belongs to C_1.

3 2D Analytical Honeycomb Geometry

3.1 Hexagonal Coordinate System

Consider the tilings in Figure 3c and 3b. As mentioned, the corresponding grids are isomorphic. An important property of these tilings is that any two non-disjoint tiles are 1-adjacent. In contrast to the case of classical rectangular grids, here 0-adjacency is impossible. Thus, a connected digital object is always 1-connected and tunnel-free. We will now develop a basis for analytical digital geometry on hexagonal grids.

We call the hexagonal tiles *2-hexels*. The centers of the 2-hexels form a sublattice L of $\mathbb{Z}^2$ whose cells are unit rhombuses (see Figure 4a). The hexels form a *digital hexagonal space*. On it, we define a *hexagonal coordinate system*. For this, we choose a hexel and define its center O to be the origin of the coordinate system. The origin's coordinates are both zeros, i.e., $O = (0, 0)$. Next we fix two coordinate axes Ob_1 and Ob_2 as shown in Figure 4a. The basis vectors $\mathbf{b_1}$ and $\mathbf{b_2}$ aligned with the coordinate axes of the system, are the vectors of the lattice basis. The so defined hexagonal coordinate system is denoted by Ob_1b_2. The coordinate axes Ob_1 and Ob_2 divide the plane into four quadrants, denoted *Quad I*, *Quad II*, *Quad III*, and *Quad IV*. The origin O is common for *Quad II* and *Quad IV*. The positive part of Ob_1 and the negative part of Ob_2 belong to *Quad IV*, while the positive part of Ob_2 and the negative part of Ob_1 belong to *Quad II*. With respect to the coordinate system Ob_1b_2, one can build an analog of the Cartesian analytical geometry.

3.2 Lines, Segments, and Polygons

Let $a_1x_1 + a_2x_2 + b = 0$, a_1, a_2, b – rational numbers, be the equation of a straight line g in the hexagonal coordinate plane. To simplify some considerations, we assume that the coefficients a_1, a_2, and b are integers and that $gcd(a_1, a_2)$ divides b. This ensures that the line g contains infinitely many equidistant lattice points. The vector $\mathbf{n} = (a_1, a_2)$ is the *normal vector* to g. The line g is collinear with the vectors $v' = (a_2, -a_1)$ and $v'' = (-a_2, a_1)$. The normal vectors to straight lines g for which the vectors v' and v'' belong to *Quad I* and *Quad III*, form an open cone C_1 (Figure 4b). Analogously, the normal vectors to straight lines g for which the vectors v' and v'' belong to *Quad II* and *Quad IV*, form a closed cone C_2 (Figure 4b). Clearly, $C_1 \cap C_2 = \emptyset$ and $C_1 \cup C_2 = \mathbb{R}^2$.

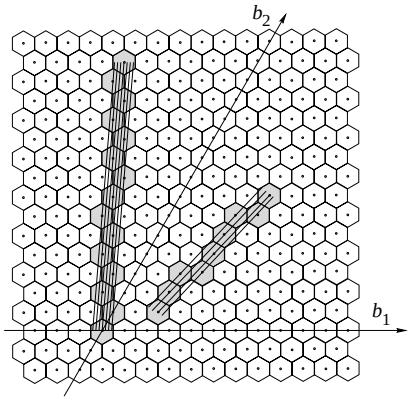

Figure 5: Two digital line segments. The one has end-points $(2,1)$ and $(4,7)$, while the other has end-points $(0,0)$ and $(-6,14)$. The normal vector to the former belongs to the cone C_1. This digital line does not have the containment property. The normal vector to the latter belongs to the cone C_2. This digital line has the containment property.

We now define a *universal digital line* corresponding to g, as follows.

$$g^D(a_1,a_2,b) = \{x \in L : 0 \le a_1x_1 + a_2x_2 + b + \lfloor t/2 \rfloor < t\},$$

where

$$t = \begin{cases} |a_1| + |a_2|, \text{ if } \mathbf{n} = (a_1,a_2) \in C_1, \\ \max(|a_1|,|a_2|), \text{ if } \mathbf{n} = (a_1,a_2) \in C_2. \end{cases}$$

See Figure 5.

The parameter t is called the *universal width* of the line g^D. It equals the number of parallel equidistant straight lines, which contain centers of hexels from g^D.

The so defined digital line g^D is *the thinnest possible* connected line of this type. For smaller values of t the line becomes disconnected, while for larger values it contains extra hexels which, however, do not influence the line connectivity. We remark that, depending on the quadrant to which the normal vector belongs, the universal width equals the thickness ω of a standard or a naive line in a square grid (see Section 2). Note also that, if $t = |a_1| + |a_2|$, then the digital line has *containment property* [9], i.e., it fully contains the corresponding continuous line. If $t = \max(|a_1|,|a_2|)$, then the containment property does not hold, in general.

Given two hexels h_1 and h_2, one can obtain a tunnel-free digital straight line segment with end-points h_1 and h_2. On this basis, one can construct tunnel-free digital polygons as a sequence of digital line segments determined by the polygon vertices.

3.3 Digital Circles

The circle is another basic Euclidean primitive admitting an easy analytical definition. In a square grid, a digital circle has been analytically defined in [1]. More precisely, one can consider the following

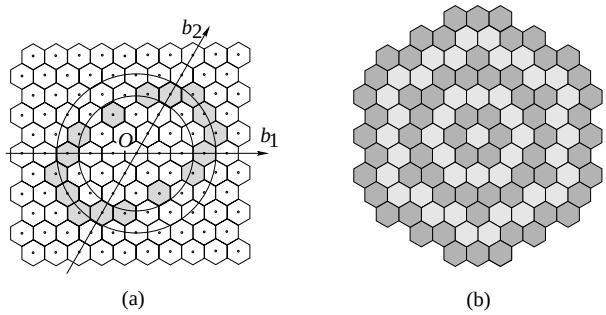

Figure 6: a) The set of hexels satisfying condition (1) with $r = 3$. b) Concentric digital circles defined by formula (2), for $r = 1, 2, 3, 4, 5$.

digital circle with center at $O(0, 0)$ and radius $r \in \mathbb{N}$.

$$C(r) = \left\{ (x, y) \in \mathbb{Z}^2 : \left(r - \frac{1}{2}\right)^2 \leq x^2 + y^2 < \left(r + \frac{1}{2}\right)^2 \right\}. \tag{1}$$

Note, however, that the above definition cannot be directly applied to a hexagonal grid since it may define a set of hexels which is too far from the intuitive idea of a circle and, in fact, can be a disconnected set of hexels (see Figure 6a). Therefore, a new definition is needed. To this end, consider a hexagonal coordinate system Ob_1b_2 with unity[3] α. We first observe that a point (x, y) of the hexagonal coordinate system has coordinates $(\alpha(x + \frac{y}{2}), \alpha\frac{\sqrt{3}}{2}y)$ with respect to the ordinary square coordinate system with unity 1, origin $(0, 0)$, and abscissa Ob_1. Then the equation of a Euclidean circle in the hexagonal system becomes

$$\alpha^2 \left(x + \frac{y}{2}\right)^2 + \alpha^2 \left(\frac{\sqrt{3}}{2}y\right)^2 = r^2, \quad \text{i.e.,} \quad \alpha^2(x^2 + xy + y^2) = r^2.$$

Thus we obtain the following analytical definition of a digital circle with center $O(0, 0)$ and radius r.

$$C^D(r) = \left\{ (x, y) \in L : \left(r - \frac{1}{2}\right)^2 \leq \alpha^2(x^2 + xy + y^2) < \left(r + \frac{1}{2}\right)^2 \right\}. \tag{2}$$

See Figure 6b. It is not hard to realize that the following properties hold.

Proposition 1 *A digital circle defined by (2) is always connected and tunnel-free. Moreover, concentric digital circles with radii $r = 1, 2, 3, \ldots$ fill the whole plane.*

3.4 Optimality of the Honeycomb Model

To have a ground for comparison between models built upon square or hexagonal grids, we suppose that the square and the hexagonal tiles have the same area 1. We call such tiles the *unit square* and the *unit 2-hexel*, respectively. It is easy to calculate that the length of a side of the unit 2-hexel is equal to $a = \frac{\sqrt{2}}{\sqrt{3}\sqrt[4]{3}} = 0.62040\ldots$.

[3]The unity α is the length of the basis vectors $\mathbf{b_1}$ and $\mathbf{b_2}$. It is easy to see that $\alpha = \sqrt{3}a$, where a is the length of a hexel side.

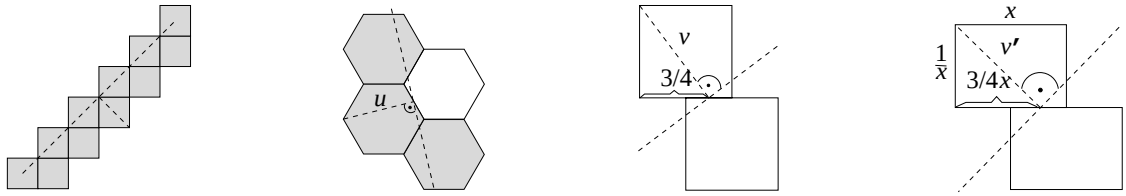

(a) (b) (c) (d)

Figure 7: Extreme cases for which a 2-hexel of a digital line has maximal deviation from the continuous line. a) In a square grid. b) In a regular hexagonal grid. c) In a regular brick-built grid. d) In the optimal brick-built grid.

3.4.1 Quality of Approximation

We show next that in certain sense the hexagonal grid provides a better approximation to a continuous line segment than the square and the brick-built grids. To this end, we first recall the definition of Hausdorff distance. Let E be a metric space with metric d, and $\mathcal{E}$ a family of closed non-empty subsets of E. For every $x \in E$ and every $A \in \mathcal{E}$ let $d(x, A) = \inf\{d(x, y) : y \in A\}$. Then, given two sets $A, B \in \mathcal{E}$, $H_d(A, B) = \max\{\sup\{d(a, B) : a \in A\}, \sup\{d(A, b) : b \in B\}\}$ is called the *Hausdorff distance* between A and B. We will suppose that d is the Euclidean metric.

We measure the *deviation* of a straight line discretization g^D from the corresponding continuous line g by the Hausdorff distance $H_d(g^D, g)$ between them.

Let us first compare the hexagonal and the square grids. As Figure 7a shows, a tunnel-free digital line might contain a pixel (or pixels) whose farthest point is in a distance $\sqrt{2} = 1.41421\ldots$ from the line. For the hexagonal grid, the maximal possible deviation is reached in the extreme case illustrated in Figure 7b. It is equal to $u = \frac{\sqrt{13}}{2}a = \frac{\sqrt{13}}{2}\frac{\sqrt{2}}{\sqrt[4]{27}} = 1.11844\ldots$, which is considerably less than in the case of square grid.

Consider now the brick-built grid whose tiles are unit squares. For it, the maximal possible deviation is reached in the case shown in Figure 7c, and is equal to $v = 1.25$. This is smaller than the corresponding value for square grid, but larger than the one for hexagonal grid.

Note that in a brick-built grid framework, unit square tiles do not provide the best possible approximation. In order to determine the dimensions of the optimal rectangle, with reference to Figure 7d, let us denote the length of its horizontal side by x. Then the other side length is $\frac{1}{x}$. Now we have to determine x which minimizes the function $f(x) = \frac{1}{x^2} + \frac{3}{4}x^2$. Using simple calculus, we find that the solution to the above optimization problem is $x = \frac{2}{\sqrt{3}} = 1.15470\ldots$. Then the other side has length $\frac{1}{x} = 0.86602\ldots$. A grid with such a tile will be called the *optimal brick-built grid*. For it, the maximal deviation is equal to $v' = \left(\left(\frac{1}{x}\right)^2 + \left(\frac{3}{4}x\right)^2\right)^{1/2} = 1.22474\ldots$. It is easy to show that the maximal deviation of a digital line in a regular hexagonal grid is minimal over all quasi-regular hexagonal grids. Similarly, the maximal deviation of a digital line in the optimal brick-built grid is minimal over all possible brick-built grids. Thus, we have obtained the following general result.

Proposition 2 *In the regular hexagonal grid the discretization of a linear object is tunnel-free. The obtained approximation is optimal over all possible uniform tilings of the plane, in terms of minimizing*

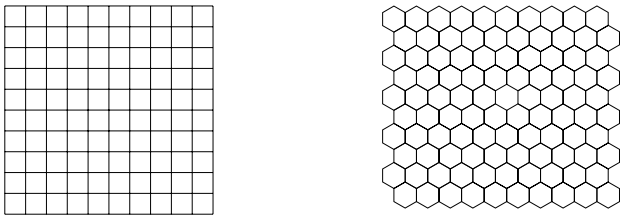

Figure 8: Illustration to Example 3.1.

the maximal possible deviation *from the continuous object.*

Similar results hold about the maximal possible deviation of a digital circle from the corresponding Euclidean circle.

3.4.2 Grid Cost

We conclude this section with one more observation, revealing that the hexagonal grid is in a sense "more economic" than the square grid. For a given grid H, the total length of all its edges is called the *cost* of H and denoted $c(H)$. One can calculate that a unit 2-hexel has perimeter $6a = 3.72241\ldots$, which is less than the perimeter of the unit square, that is 4. This fact may have an advantageous impact on the cost of the corresponding grid, as illustrated through the following example.

Example 1 Consider the grid of a screen with a square shape, consisting of n rows, each of them containing n unit tiles. Consider the square grid H_1 (Figure 8a) and hexagonal grid H_2 (Figure 8b). Both grids cover the same area n^2. One can easily find that in the former case the grid cost is $c(H_1) = 2n^2 + 2n$, while in the latter case it is $c(H_2) = (3n^2 + 4n - 1)a = (3a)n^2 + 4an - a$. Since the coefficient of n^2 in $c(H_2)$ is $3a = 1.86120... < 2$, we obtain that $c(H_2)$ is asymptotically smaller than $c(H_1)$.

It is easy to show that a unit 2-hexel has a minimal perimeter among all quasi-regular hexagons with area 1. One can also show that a tiling by unit 2-hexels has minimal cost among all possible tilings by quasi-regular hexagons with area 1. Similarly, a unit square has a minimal perimeter among all parallelograms with area 1, and a tiling by a unit square has a minimal cost over all possible tilings by parallelograms with area 1. Thus, one can conclude that the tiling with regular hexagons has minimal cost over all possible uniform tilings. This property may be of interest regarding possible wire grid fabrication for the purpose of a novel computer screen design, based, e.g., on liquid-crystals, plasma panels, or electro-luminescent technologies.

4 3D Honeycomb Geometry

In this section we present two 3D honeycomb models and related analytical digital geometry. In both of them the 3D space is tiled by a right hexagonal prism called 3-hexel. The base of the prism is a unit 2-hexel and its height has length 1. Thus the 3-hexel volume is equal to 1.

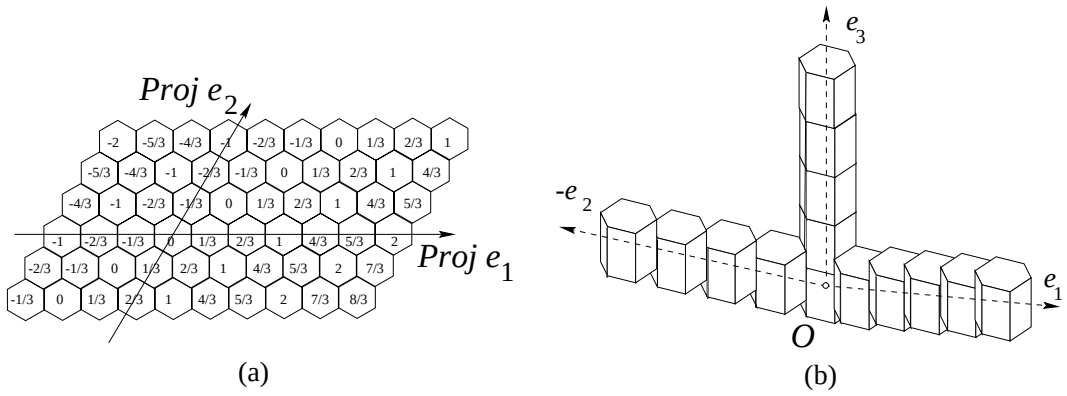

Figure 9: Illustration to Model I. a) The orthogonal projections of the centers of 3-hexels on the plane $\mathcal{P}$. b) The axes of the coordinate system $Oe_1e_2e_3$. The rays e_1 and $-e_2$ make an angle of 120 degrees.

Our aim is to create a basis for tunnel-free discretizations of surfaces, in particular of planes and spheres. For this, we consider two special tilings of $\mathbb{R}^3$ by 3-hexels and define corresponding coordinate systems in them.

4.1 Model I

Let h_0 be a 3-hexel in $\mathbb{R}^3$. We assign to its center O coordinates $(0, 0, 0)$ and consider it as the origin of a coordinate system. Consider a tiling of $\mathbb{R}^3$ as the one illustrated in Figure 9a,b. The figure exposes the orthogonal projections of the centers of a set of 3-hexels on the plane $\mathcal{P}$, passing through the origin O and orthogonal to the hexel's height. The tiling has the property that the third coordinates of two side-neighboring 3-hexels differ either by $\frac{1}{3}$ or by $\frac{2}{3}$. Thus any two neighboring hexels are 2-adjacent. We choose as a third coordinate axis the ray e_3 passing through O and orthogonal to $\mathcal{P}$. On every hexagonal projection the third coordinate of the corresponding 3-hexel's center is marked (i.e., the coordinate of the hexel's center with respect to the e_3 axes). These centers belong to a plane which is chosen to be one of the digital coordinate planes. In it, we fix the other two coordinate axes e_1 and e_2, as illustrated in Figure 9. The origin O and the axes e_1, e_2, and e_3 determine the coordinate system $Oe_1e_2e_3$.

Now for each 3-hexel h from the digital coordinate plane Oe_1e_2, we tile the space upward and downward by adjacent copies of h. Thus, we obtain a tiling of $\mathbb{R}^3$, which defines a digital honeycomb space. In the digital coordinate plane Oe_1e_2 one can consider the four quadrants $QuadI$, $QuadII$, $QuadIII$, and $QuadIV$, determined by the coordinate axes.

By construction, the centers of the 3-hexels form a lattice H in $\mathbb{R}^3$ whose cells are parallelepipeds. Its basis vectors $\mathbf{e_1}$, $\mathbf{e_2}$, and $\mathbf{e_3}$ are also basis vectors for the coordinate system $Oe_1e_2e_3$. We denote by α the length of $\mathbf{e_1}$ and $\mathbf{e_2}$ and by β the length of $\mathbf{e_3}$. Note that α and β may be different. As in the 2D case, $\alpha = \sqrt{3}a$, where a is the length of the side of a hexagonal face. In general, β may be an arbitrary positive real number. If $a = \frac{\sqrt{2}}{\sqrt{3}\sqrt[4]{3}}$, then the 3-hexel's hexagonal face has area 1. If, in addition, $\beta = 1$, then the 3-hexel has volume 1.

Note that every two neighboring 3-hexels are 2-adjacent. No 0- or 1-tunnel is possible in a

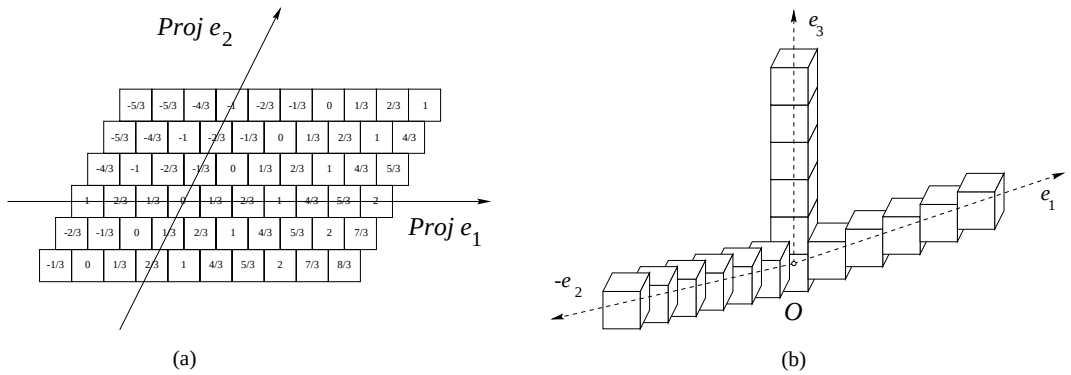

Figure 10: Illustration to a brick-built version of model I.

connected set of 3-hexels.

As in dimension two, one can consider brick-built versions of the model, where the hexagonal prisms are substituted by rectangular prisms (see Figure 10).

4.1.1 Analytical Digital Plane

Consider a Euclidean plane P with equation $a_1x_1 + a_2x_2 + a_3x_3 = b, \quad a_1, a_2, a_3, b \in \mathbb{Z}$ with respect to the defined coordinate system. Assume as before that $gcd(a_1, a_2, a_3)$ divides b, i.e., P contains a 2-dimensional lattice L which is a sublattice of H.

We define a *universal digital plane* corresponding to P, as follows:

$$P^D(a_1, a_2, a_3, b) = \{x \in H : 0 \leq a_1x_1 + a_2x_2 + a_3x_3 + b + \lfloor t/2 \rfloor < t\}, \tag{3}$$

where

$$t = \begin{cases} |a_1| + |a_2| + |a_3|, \text{ if } \mathbf{n} = (a_1, a_2) \in C_1, \\ \max(|a_1|, |a_2|, |a_3|), \text{ if } \mathbf{n} = (a_1, a_2) \in C_2. \end{cases}$$

C_1 and C_2 are cones in the coordinate plane Oe_1e_2 defined as in the 2D case. The parameter t is called the *universal width* of the plane P^D.

By the construction of the digital space, the so defined digital plane is always tunnel-free and appears to be the thinnest possible tunnel-free digital plane of this type. Similar to the 2D case, planes with thickness $t = |a_1| + |a_2| + |a_3|$ possess the containment property, while those with thickness $t = \max(|a_1|, |a_2|, |a_3|)$, in general, don't.

4.1.2 Digital Spheres

In the cubic model, an analytical digital sphere with center $O(0, 0, 0)$ and radius $r \in \mathbb{N}$ is defined as follows [1]:

$$C(r) = \left\{(x, y, z) \in \mathbb{Z}^3 : \left(r - \frac{1}{2}\right)^2 \leq x^2 + y^2 + z^2 < \left(r + \frac{1}{2}\right)^2\right\}. \tag{4}$$

In order to obtain a reasonable definition within the considered honeycomb model, we have to make certain relevant transformations. Consider a honeycomb coordinate system $Oe_1e_2e_3$ whose basis vectors

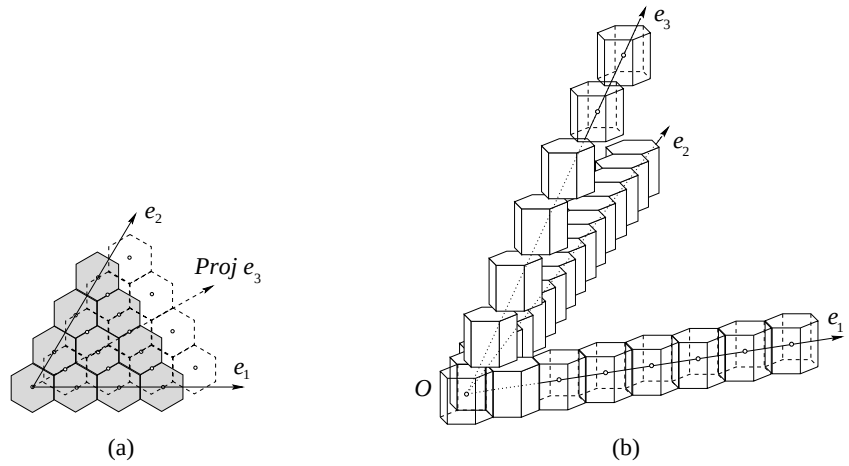

Figure 11: Illustration to Model II. a) Projections of two consecutive slices of 3-hexels on the coordinate plane Oe_1e_2. b) The axes of the coordinate system $Oe_1e_2e_3$.

$\mathbf{e_1}$ and $\mathbf{e_2}$ have length α, while the third basis vector $\mathbf{e_3}$ has length β. It is not hard to compute that a point (x, y, z) of the honeycomb coordinate system has coordinates $\left(\alpha(x + \frac{y}{2}), \alpha\frac{\sqrt{3}}{2}y, \frac{1}{3}x - \frac{1}{3}y + \beta z\right)$ with respect to a cubic coordinate system $Oe_1'e_2'e_3'$ with unity 1, centered at $O(0, 0, 0)$, and such that the projection of the basis vector $\mathbf{e_1}$ over the coordinate plane $Oe_1'e_2'$ has z-coordinate $\frac{1}{3}$, and the projection of the basis vector $\mathbf{e_2}$ over $Oe_1'e_2'$ has z-coordinate $-\frac{1}{3}$. Then the equation of a Euclidean sphere in the honeycomb coordinate system is

$$\alpha^2\left(x + \frac{y}{2}\right)^2 + \frac{3}{4}\alpha^2y^2 + \left(\frac{1}{3}x - \frac{1}{3}y + \beta z\right)^2 = r^2,$$

or, equivalently,

$$\left(\alpha^2 + \frac{1}{9}\right)x^2 + \left(\alpha^2 + \frac{1}{9}\right)y^2 + \beta^2z^2 + \left(\alpha^2 - \frac{2}{9}\right)xy + \left(\frac{2}{3}\beta\right)xz - \left(\frac{2}{3}\beta\right)yz = r^2.$$

This equation implies a definition of a digital honeycomb sphere. Its properties parallel those of a digital circle in the plane (see Proposition 1).

4.2 Model II

Consider a regular hexagonal tiling of the plane. On every tile we build the corresponding 3-hexel. Thus we obtain a digital 3D plane P_0. We fix one of its hexels and choose its center $O(0, 0)$ to be the origin of a coordinate system. Then we define the axes e_1 and e_2 as in the 2D case. Thus we obtain a digital coordinate plane Oe_1e_2. We now build on top of P_0 another equivalent "slice" of 3-hexels, shifted as illustrated in Figure 11a. Proceeding analogously upward and downward, we obtain a tiling of $\mathbb{R}^3$. The tiles' centers constitute a lattice in $\mathbb{R}^3$ whose cells are parallelepipeds. We determine the third axis e_3 as shown in Figure 11b. The basis vectors of the coordinate system are the basis vectors $\mathbf{e_1}$, $\mathbf{e_2}$, and $\mathbf{e_3}$ of the underlying lattice. The length of $\mathbf{e_1}$ and $\mathbf{e_2}$ is equal to $\alpha = \sqrt{3}a$, and the length

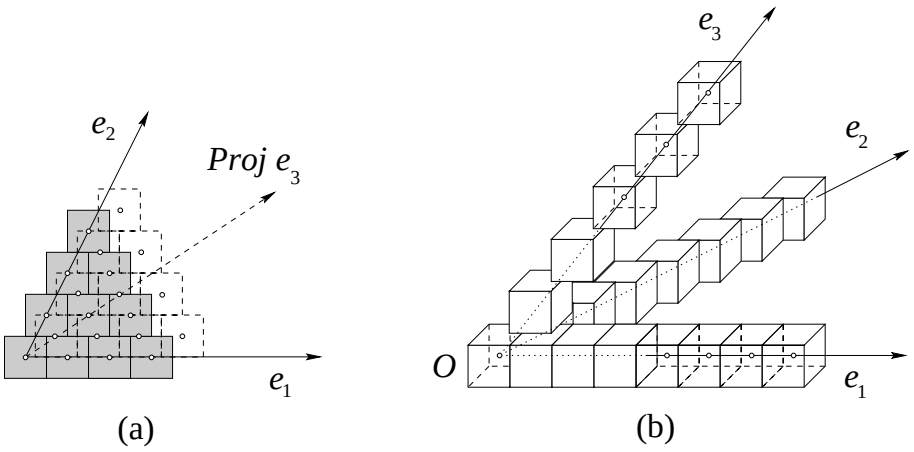

Figure 12: Illustration to a brick-built version of Model II.

β of $\mathbf{e_3}$ is a positive real number satisfying the condition $\beta > \frac{3}{4}a$. (This last inequality implies that the hexagonal prism tile has positive height.)

The brick-built version of Model II is illustrated in Figure 12.

Similar to Model I, a connected set of 3-hexels is always 2-connected and does not contain any 0- and 1-tunnels. Moreover, within both models the adjacency relation μ defined by nearest neighbor forms a good pair (μ, μ).

4.3 Digital Planes and Spheres

In the constructed digital space, formula (3) defines a digital plane in the same way as within Model I. It is always tunnel-free and appears to be the thinnest possible tunnel-free digital plane of this type. One can also show that a digital plane defined by (3) provides a better approximation to the corresponding continuous plane (in terms of maximal deviation from the continuous plane) than the corresponding standard plane within the cubic model.

Digital sphere is defined analogously to Model I. It is not hard to calculate that within Model II, the equation of a sphere with center $O(0,0,0)$ and radius r is

$$\alpha^2 x^2 + \alpha^2 y^2 + \left(\frac{9}{4}a^2 + \beta^2\right) z^2 + \alpha^2 xy + \left(\frac{3\sqrt{3}}{2}\alpha a\right) xz + \left(\frac{3\sqrt{3}}{2}\alpha a\right) yz = r^2,$$

which immediately implies an analytical definition of a digital sphere. Its properties are similar to those of the digital circle given in Proposition 1.

4.4 Uniqueness of Model I and Model II

In this section we further study the structure of a 3-hexel neighborhood in Model I and Model II. In both models the geometric position of two neighboring hexels is strictly fixed. In Model I, the z-coordinates of any two hexels differ by integer multiple of $\frac{1}{3}$ (see Figure 9). In Model II, the digital space consists of "slices," shifted in such a way that the orthogonal projection of a hexel's center

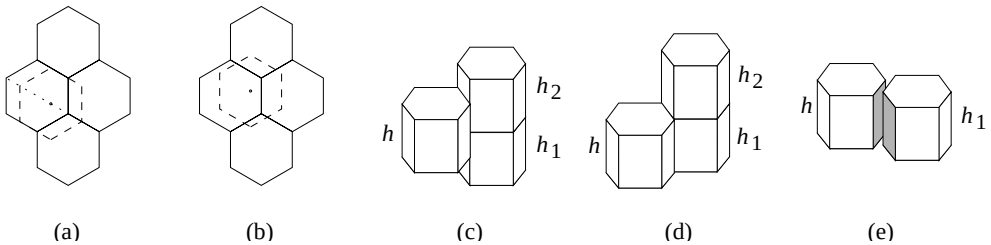

Figure 13: a) The orthogonal projection of a hexel's center over the lower slice belongs to a diagonal of a hexagon. b) The orthogonal projection of a hexel's center over the lower slice in a feasible modification of Model I. c), d), e) Illustrations to the proof of Proposition 3.

over the coordinate plane Oe_1e_2 falls exactly in the middle of a side of a hexagonal hexel's face from the lower slice (see Figure 11). Note that these models can be changed to a certain extent, so that the obtained tilings still be uniform and any two adjacent tiles be 2-adjacent. For instance, in the framework of Model II, these properties would be preserved if two consecutive slices are shifted in any arbitrary manner, unless the projection of a hexel's center falls on a diagonal of a hexagonal hexel's face from the lower slice (see Figure 13a,b). Model I admits various modifications, as well. One can see that all modifications preserving the required properties must satisfy the following conditions.

1. In Model I, every 3-hexel of the 3D digital space has one 2-neighbor for the upper hexagonal face, one for the lower hexagonal face, and two for each one of the six side rectangular faces.

2. In Model II, there are four neighbors for every one of the two hexagonal faces and one for each of the six rectangular faces.

Modifications of Model I and Model II satisfying the above conditions will be called *feasible*. Note that although the structure of a 3-hexel neighborhood in feasible modifications of Model I and Model II is quite different, in both models a 3-hexel has the same number of neighbors (i.e., 14).

We now show that the neighborhood structures relative to Model I and Model II are the only possible, under the condition that the tiling is uniform and any two adjacent tiles are 2-adjacent. Consider a 3-hexel h. The following two cases are possible. *Case 1:* Any hexagonal face of h is 2-adjacent to exactly one hexagonal face of another 3-hexel; *Case 2:* Any hexagonal face of h is 2-adjacent to exactly four hexagonal faces of four other 3-hexels. (Clearly, a hexagonal face of h cannot be covered by two hexels only. If this is done by three hexels, then in the tiling there must be pairs of hexels which share a single vertex. This would contradict the condition that any two adjacent tiles are 2-adjacent.)

Consider Case 1. We have that every one of the rectangular side faces of h is 2-adjacent to exactly two 3-hexels h_1 and h_2, as h_2 is on top of h_1 and the vertical edges of h, h_1 and h_2 are aligned (see Figure 13c). To see this, assume by contradiction that h is 2-adjacent only to h_1 and shares a common rectangular face with it. Then h and h_2 share an edge (Figure 13d) and there is a 1-tunnel between h and h_2 - a contradiction. Now assume that the vertical edges of h and of its neighbor h_1 are not aligned (see Figure 13e). Then clearly $\mathbb{R}^3$ cannot be tiled by a 3-hexel, since the space angle between some faces of h and h_1 will equal 60 degrees, which is a contradiction. Similar reasoning

(a) (b)

Figure 14: a) The point B is in a distance $\sqrt{3}$ from the Euclidean plane passing through the point A and orthogonal to the straight line AB. b) The diagonal PQ of a 3-hexel is shorter than the one of the unit cube which equals $\sqrt{3}$.

shows that in Case 2, every rectangular side face of h will be shared with another 3-hexel. Thus we obtain the following result.

Proposition 3 *The two neighborhood structures relative to feasible modifications of Model I and Model II are the only ones possible, under the condition that the tiling is uniform and any two adjacent tiles are 2-adjacent.*

4.5 Optimality Issues

Let us define a grid cost in a 3D model as the total area of the surfels (faces) of the tiles included in certain volume (e.g., in a cube with a side n). We notice that the area of a 3-hexel is equal to $2\times 1+6\times a = 2+3.72241... = 5.72241...$, which is less than the one of the unit cube, that is 6. Similar to the case of a 2D hexagonal grid, this implies that the grid cost in a honeycomb model is lower than the one in the cubic model.

More importantly, the definition of a digital plane within Model I and Model II ensures better approximation to the continuous plane (in terms of maximal possible deviation) compared to the classical cubic model. In fact, a tunnel-free standard plane may contain voxels that are in a distance $\sqrt{3}$ from the continuous plane (see Figure 14a), while within Model I and Model II this distance is clearly smaller. This can be immediately deduced from the fact that the longest diagonal of a 3-hexel equals $f = (1+(2a)^2)^{1/2} = 1.59361\ldots$, which is less than $\sqrt{3} = 1.73205\ldots$ (see Figure 14b). It is not hard to show that tiling by a right prism with a regular hexagonal base provides better approximation than a tiling by a prism which is inclined and/or with a quasi-regular hexagonal base.

Similar considerations and conclusions hold for the case of brick-built models (see Figure 10 and Figure 12). One can show that with respect to the value of the maximal possible deviation from the continuous plane, the honeycomb models I and II are superior to the corresponding brick-built models, while the latter are superior to the cubic model.

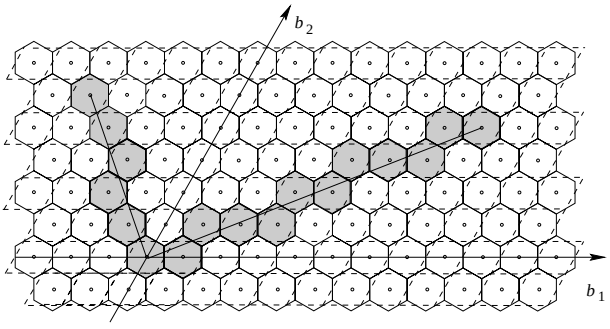

Figure 15: Hexagonal digital space with two digital line segments in it, together with the corresponding rhomboidal digital space.

5 Algorithmic and Complexity Issues

The considered analytical discrete primitives (digital straight lines and line segments, digital circles, planes, and spheres) admit an efficient algorithmic generation, which can be performed in time that is linear in the number of the generated hexels. To show this, below we explain how *everyone* of the well-known linear time classical algorithms can be straightforwardly adapted to the honeycomb model. For the sake of simplicity, we consider the problem of digital straight line generation.

Let g^D be a 2D digital line in the 2D digital hexagonal space. Any 2-hexel corresponds to a rhombus with the same center and with sides determined by the basis vectors of the space Ob_1b_2 (see Figure 15). This correspondence defines a rhomboidal digital space $\overline{Ob_1b_2}$ with the same center and basis vectors, as shown in Figure 15. In it, the rhombuses with centers corresponding to hexels form the given digital line g^D constitute a digital line $\bar{g}$. If the normal vector $\mathbf{n}$ to the continuous line g belongs to the cone C_1, then $\bar{g}$ is a standard digital line in $\overline{Ob_1b_2}$. If $\mathbf{n} \in C_2$, $\bar{g}$ is a naive line in $\overline{Ob_1b_2}$. These digital lines can be constructed by the well-known linear-time algorithms for standard or naive line generation (see, e.g., [21]). Because of the one-to-one correspondence between 2-hexels and rhombuses, we also obtain the centers of the hexels of the honeycomb digital line. Thus the time-complexity of honeycomb digital line generation matches the time-complexity of the algorithms for standard/naive line generation, depending on the cone to which the normal vector $\mathbf{n}$ belongs. Note that if $\mathbf{n} \in C_2$, we have to construct a naive line in the rhomboidal model. In this case the algorithm efficiency will be superior to the one for standard line generation within the classical square model.

The above considerations easily extend to both 3D honeycomb models of Section 5.1 and 5.2. Since in these models the hexels' centers form lattices, any 3-hexel h corresponds to a parallelepiped which has the same center as h and whose upper and lower faces are portions of planes containing the two hexagonal faces of h. Thus we obtain a 3D digital space $\overline{Oe_1e_2e_3}$ with the same center and basis as $Oe_1e_2e_3$, whose cells are parallelepipeds. In this new space, one can search a plane discretization applying the well-known algorithms for standard or naive plane generation, depending on the cone to which the projection of the normal vector belongs.

6 Concluding Remarks

In this paper we have developed analytical digital geometry for raster and volume graphics based on a hexagonal grid (resp. hexagonal prism tilings). In particular, we have defined digital lines and circles (in the 2D space) and digital planes and spheres (in the 3D space). We have also observed that the honeycomb models ensure discretizations which are in some regards superior to the classical ones.

One can develop methods for discretizing more sophisticated objects (especially in $\mathbb{R}^3$), like 3D line segments, polygons and meshes of polygons. For this, one can appropriately modify certain discretization schemes and algorithms, which have been developed for classical square/cubic models (see, e.g., [28, 6, 8, 7]). Note that some problems that required long and complicated solutions within the cubic model [6, 8], can be handled more easily within the honeycomb models. Thus in various regards the honeycomb models can serve as a useful alternative to the classical approaches in raster and volume modeling.

Acknowledgements

We thank Eric Andres, Claudio Montani, Roberto Scopigno, and Marco Pellegrini for reading early versions of this paper and making comments and suggestions. We are grateful to Gabor Herman and Edgar Garduno for a useful discussion on the possible wealth of using non-cubic models. The first author thanks Reinhard Klette for a number of interesting discussions.

References

[1] Andres, E. (1992) *Cercles Discrets et Rotations Discrètes.* Thèse de Doctorat, Centre de Recherche en Informatique, Université Louis Pasteur, Strasbourg, France.

[2] Andres, E. (2001) *Modélisation Analytique Discrète d'Objets G''eometriques.* Thèse de habilitation à diriger des recherches, Universit''e de Poitiers, Poitiers, France.

[3] Andres, E., Achatya, R. and Sibata, C. (1997) The discrete analytical hyperplane. *Graphical Models and Image Processing*, **59**(5), 302–309.

[4] Andres, E., Nehlig, P. and Françon, J. (1997) Tunnel-free supercover 3D polygons and polyhedra. In Fellner, D. and Szirmay-Kalos (eds) *Eurographics'97*, Vol. **16**(3), C3–C13, Blackwell Publishers, Oxford–Malden.

[5] Brimkov, V.E., Andres, E. and Barneva, R. (2002) Object discretizations in higher dimensions. *Pattern Recognition Letters*, **23**(6), 623–636.

[6] Barneva, R.P., Brimkov, V.E. and Nehlig, Ph. (2000) Thin discrete triangular meshes. *Theoretical Computer Science*, **246** (1-2), 73–105.

[7] Brimkov, V.E. and Barneva, R. (2002) Graceful planes and lines. *Theoretical Computer Science*, **283**, 151–170.

[8] Brimkov, V.E., Barneva, R. and Nehlig, Ph. (2000) Minimally thin discrete triangulations. In Chen, M., A. Kaufman, A. and Yagel, R. (eds), *Volume Graphics*, Springer Verlag, London.

[9] Cohen, D. and A. Kaufman, A. (1997) 3D Line voxelization and connectivity control. *Proceedings CG&A'97*, 1–24.

[10] Debled-Rennesson, I., Reveillès, J-P. (1994) A new approach to digital lines. *Proceedings of SPIE's International Symposium on Photonics for Industrial Applications "Vision Geometry 3"*, Boston, USA.

[11] Figueiredo, O., Reveillès, J-P. (1995) A contribution to 3D digital lines. *Proceedings of the 5th International Workshop on Discrete Geometry for Computer Imagery*, Clermont-Ferrand, 187–198, Springer-Verlag, Berlin.

[12] Françon, J. (1996) On recent trends in discrete geometry in computer imagery, *Proceedings of the 6th International Workshop on Discrete Geometry for Computer Imagery*, Lyon, Lecture Notes in Computer Science No 1176, Springer-Verlag, 141–150.

[13] Garduno, E., *Visualization and Extraction of Structural Components from Reconstructed Volumes.* (2002) Ph.D. Thesis, University of Pennsylvania, USA, 2002.

[14] Gomes, J. and Velho, L. (1997) *Image Processing for Computer Graphics.* Springer Verlag, New York.

[15] Herman, G. (1998) *Geometry of Digital Spaces.* Birkhäuser, Boston.

[16] Johnson, E.G., Rosenfeld, A. (1970) Geometrical operations on digital pictures. In Lipkin, B.S. and A. Posenfeld, A. (eds), *Picture Processing and Psychopictorics*, Academic Press, New York.

[17] Kaufman, A., Cohen, D. and Yagel, R. (1993) Volume graphics, *IEEE Computer*, **26**(7), 51–64.

[18] Kong, T.Y. (2001) Digital topology. In Davis, L.S. (ed), *Foundations of Image Understanding*, Kluwer, Boston, Massachusetts.

[19] Kong, T.Y., Rosenfeld, A. (1989) Digital topology: introduction and survey. *Computer Vision, Graphics and Image Processing*, **48**, 357–393.

[20] Miller, E.G. (1999) Alternative tilings for improved surface area estimates by local counting algorithms. *Computer Vision and Image Understanding*, **74**, 193–211.

[21] Reveillès, J.-P. (1991) *Géométrie Discrète, Calcul en Nombres Entiers et Algorithmique.* Thèse d'État, Université Louis Pasteur, Strasbourg, France.

[22] Rogers, C.A. (1964) *Packing and Covering.* Cambridge University Press, Cambridge.

[23] Rosenfeld, A. (1998) Digital geometry – history and open problems. In Rosenfeld, A. and Sloboda, F. (eds), *Advances in Digital and Computational Geometry.* Springer, Singapore.

[24] Rosenfeld, A. (1973) Arcs and curves in digital pictures. *Journal of the ACM*, **18**, 81–87.

[25] Klette, R. and Rosenfeld, A. (2004) *Digital geometry. Geometric methods for digital picture analysis.* Morgan Kaufmann Publishers, San Francisco.

[26] Saha, P., and Rosenfeld, A. (1998) Strongly normal sets of convex polygons or polyhedra. *Pattern Recognition Letters*, **19**, 1119–1124.

[27] Sonka, M., Hlavac, V. and Boyle, R. (1998) *Image Processing, Analysis, and Machine Vision* (2nd Edition), IT Pu. Co.

[28] Stojmenovic, I. and Tosic, R. (1991) Digitization schemes and the recognition of digital straight lines. Hyperplanes and flats in arbitrary dimensions. *Digital Geometry*, Contemporary Math. Series, Amer. Math. Soc., Providence, RI, **119**, 197–212.

[29] Voss, K., (1993) *Discrete Images, Objects, and Functions in* $\mathbf{Z}^n$. Springer, Berlin.

[30] Wuthrich, C.A. and Stucki, P. (1991) An algorithm comparison between square- and hexagonal-based grids. *Graphical Models and Image Processing*, **53**(4), 324–339.

[31] Yong-Kui, L. (1993) The Generation of Straight Lines on Hexagonal Grids. *Computer Graphics Forum*, **12**(1), 21–25.

[32] Yong-Kui, L. (1993) The Generation of Circular Arcs on Hexagonal Grids. *Computer Graphics Forum*, **12**(1), 27–31.